

Resonant Triads Involving a Nondispersive Wave

By Rodolfo R. Rosales, Esteban G. Tabak, and Cristina V. Turner

A simple system is studied, involving a single nondispersive breaking wave and its interaction with two dispersive modes through a resonant triad. The dynamics of this system are shown to be quite rich, through a combined theoretical and numerical analysis. A sharply defined traveling wave with a corner seems to attract almost all initial data with enough energy, provided the nondispersive wave is unstable to the other two when standing alone. In other cases, the solution converges to quasiperiodic final states, unless extra symmetries force the solution to converge to simpler configurations.

1. Introduction

In the world of wave motion, a sharp distinction exists between *dispersive* and *nondispersive* waves. At the linear level, the former decompose any initial disturbance into its elementary sinusoidal mode components, each mode traveling at its own individual group velocity, while the latter preserve the shape of initial disturbances forever, with all modes traveling together as a pack. At the outset of nonlinearity, this difference in linear behavior gives rise to mode interactions of a very different character. Because the various modes of a nondispersive wave travel together for long periods, they can exchange energy rather strongly, yielding a nonlinear modulation of the wave's shape, which, in

Addresses for correspondence: Professor R. R. Rosales, Department of Mathematics, Room 2-330, MIT, Cambridge, MA 02139. E-mail: rrr@math.mit.edu; and Professor E. G. Tabak, Department of Mathematics, Courant Institute of Mathematics, NYU, 251 Mercer Street, New York, NY 10012. E-mail: tabak@cims.nyu.edu.

most situations involving waves in fluids, leads to wave breaking and shock formation. Dispersive modes, in contrast, overlap only over relatively short periods, so the nonlinear energy exchange among them is highly reduced. The only exception to this rule is given by *resonance*: When a set of modes, say three, is such that the relative phase between the product of two of them and the remaining one does not change over time, energy exchanges within the set are again rather strong.

In fluids, the slow modulation of nondispersive waves is often described in terms of an inviscid Burgers' equation. The resonant interaction within a triad of dispersive modes can be modeled by a set of ordinary differential equations with Hamiltonian structure and enough constants of motion that they can be fully integrated in terms of elliptic functions. When many resonant or near-resonant triads are present, on the other hand, the solutions are much less organized, to the point of requiring a statistical treatment. Systems that are only weakly dispersive, as free surface waves over shallow but finite depths, yield reduced equations in the spirit of the Korteweg–de Vries equation [1].

However, often both dispersive **and** nondispersive waves are solutions of a single system. An example is provided by Kelvin waves, both coastal and equatorial, which live as isolated nondispersive waves in a “dispersive sea,” which includes inertial and planetary waves. When this is the case, the two canonical forms of nonlinear mode interaction get blended together, producing novel dynamics, which include shocks and smooth traveling waves, with ubiquitous waves presenting corner singularities in between these two extremes [2].

In this article, we explore one of the simplest possible blends of dispersive and nondispersive effects: a nondispersive wave, with Burgers-like self-interactions conducive to breaking, with one mode coupled to two dispersive wave modes through a triad resonance. A similar study where one of the dispersive modes was replaced by topography was conducted in [2]. A curious tendency was observed there for nearly all initial data to converge to shockless solutions with corners, either a well-defined traveling wave, when the initial data have enough energy, or a quasiperiodic wave, for less energetic initial data. These results are very similar to those investigated in [3–6] for purely hyperbolic waves, such as those arising in gas dynamics, interacting through a variable medium or an inhomogeneous entropy.

In the case of interest here with a full triad, a new question arises. It is well known that, for regular triads, the steady solutions in which only one element of the triad is excited are stable or unstable, depending on whether or not the frequency of the corresponding mode agrees in sign with one of the other two. It has often been speculated that this stability criterion carries through to more complicated scenarios, where none of the waves is zero, determining a direction of energy flow through the triad [7]. In our context here, we would like to determine whether which of the three waves is the “unstable” one, the

nondispersive, or one of the dispersive ones, has any significant effect on the dynamics of the system. In particular, we would like to discover whether the strong convergence of high-energy initial data to traveling waves with a corner occurs independently of the relative signs of the three frequencies involved.

2. The resonant equations and their conserved quantities

We consider the system

$$u_t + \left(\frac{1}{2} u^2 \right)_x = 2\operatorname{Re} \left(i k a b e^{-i k x} \right), \quad (1)$$

$$a_t = -i \omega_a \overline{b \hat{u}_k}, \quad (2)$$

$$b_t = -i \omega_b \overline{a \hat{u}_k}, \quad (3)$$

where $u = u(x, t)$ is the nondispersive wave amplitude (real valued, 2π -periodic in space and normalized to zero mean), $a = a(t)$ and $b = b(t)$ are the (complex) amplitudes of the dispersive waves, ω_a and ω_b are the corresponding dispersive wave frequencies, the bars represent complex conjugation, \hat{u}_k is the k th Fourier coefficient of u (for some integer k),

$$\hat{u}_k(t) = \frac{1}{2\pi} \int_0^{2\pi} u(x, t) e^{-i k x} dx,$$

and the condition for resonance,

$$k + \omega_a + \omega_b = 0,$$

is satisfied.

This system arises as a reduced asymptotic model for the nonlinear interaction between three waves: one nondispersive and two dispersive, the latter in resonance with one mode of the former. Physical examples include wave dynamics in the equatorial wave guide, where a nondispersive Kelvin wave may exchange energy resonantly with either Rossby, Yanai, or Poincaré waves.

Typically, in an asymptotic derivation of the equations, t is a slow time, $t = \epsilon T$, where $0 < \epsilon \ll 1$ is the nonlinear strength, and T is the fast “real” time. Similarly, x represents the phase of the nondispersive wave, $x = X - cT$, where c (taken equal to 1 here for concreteness) is the linear speed of the nondispersive wave, and X is the space coordinate in a fixed frame of reference. To leading order, the full waves have the form

$$\begin{aligned} U(X, T) &= u(x, t), \\ A(X, T) &= a(t) e^{i k_a X - i \omega_a T}, \\ B(X, T) &= b(t) e^{i k_b X - i \omega_b T}, \end{aligned} \quad (4)$$

with the additional resonance condition $k_a + k_b + k = 0$. For the k th mode in the nondispersive wave, we have:

$$\begin{aligned}\frac{d\hat{u}_k}{dt} &= -i k \overline{a b} + \text{NSIT}, \\ \frac{da}{dt} &= -i \omega_a \overline{b \hat{u}_k}, \\ \frac{db}{dt} &= -i \omega_b \overline{a \hat{u}_k},\end{aligned}\tag{5}$$

where NSIT (Nonlinear Self-Interaction Terms) are the terms generated by $(\frac{1}{2}u^2)_x$ in (1), arising from the nonlinear coupling among all modes of the nondispersive wave. If we ignore these terms, (5) is the standard form of the reduced interaction equations for three resonant waves.

The system (1–3) is Hamiltonian, with Hamiltonian

$$H = \frac{1}{12\pi} \int_0^{2\pi} u^3 dx + 2\text{Re}(a b \hat{u}_k).\tag{6}$$

The Hamiltonian form of the equations is

$$\begin{aligned}u_t &= -\frac{\partial}{\partial x} \frac{\delta H}{\delta u}, \\ a_t &= -i \omega_a \frac{\delta H}{\delta \bar{a}}, \\ b_t &= -i \omega_b \frac{\delta H}{\delta \bar{b}}.\end{aligned}\tag{7}$$

This Hamiltonian form is valid only as long as the solution remains smooth. When shocks develop, the Hamiltonian is no longer a conserved quantity and it starts to evolve according to the equation

$$\frac{dH}{dt} = \sum_{\text{shocks}} \frac{1}{4\pi} \left(\frac{s}{3} [u^3] - \frac{1}{4} [u^4] \right),$$

where the brackets stand for the magnitude of the jumps in the enclosed variables across the shocks (value behind minus value ahead), and s is the shock speed. However, the Hamiltonian does not have a definite sign. A (probably) more relevant *wave energy* is given by

$$E(t) = \int_0^{2\pi} \frac{1}{2} u^2 dx + 2\pi(|a|^2 + |b|^2).\tag{8}$$

The positive definite quantity $E(t)$ is conserved while the solution remains smooth, and becomes monotone decreasing when shocks are present, the rate of change then given by

$$\frac{dE}{dt} = - \sum_{\text{shocks}} \frac{1}{12} [u]^3 < 0.$$

Here the inequality follows from the *Entropy Condition* $[u] > 0$, that must apply across shocks. In addition, the following (Manley–Rowe) quadratic form is always conserved, with or without shocks:

$$Q = \omega_a |b|^2 - \omega_b |a|^2.$$

The nature of this invariant, which depends on the signs of ω_a and ω_b , will be shown below to affect significantly the nature of the solutions to the system in (1–3).

Two other invariants (modulus dissipation at shocks) can be found by combining E and Q :

$$Q_{ea} = \frac{1}{2\pi} \int_0^{2\pi} \frac{1}{2} u^2 dx - \frac{k}{\omega_a} |a|^2$$

and

$$Q_{eb} = \frac{1}{2\pi} \int_0^{2\pi} \frac{1}{2} u^2 dx - \frac{k}{\omega_b} |b|^2.$$

The three invariants Q , Q_{ea} , and Q_{eb} are instrumental in proving the following stability criterion. Consider a state where only one of $u(x)$, a and b is nonzero. Such a state is stable unless the nonzero mode is the one associated with a frequency (k , ω_a , or ω_b) of sign opposite to the other two (for otherwise, the Manley–Rowe invariant associated with the other two modes is positive definite, so these modes cannot, even nonlinearly, depart from zero.) Hence, this criterion distinguishes one of the three modes as unstable to the other two, which raises the question of whether this mode being u , or one of a and b has any significant effect on the dynamics of the system in situations where all three waves are nonzero.

3. Some exact solutions

The equations (1–3) have some interesting exact solutions that play a fundamental role in their dynamics, as we show in the numerical simulations below. First, we seek traveling waves of the form

$$u(x, t) = F(x - st), \quad (9)$$

where s is an arbitrary constant. For concreteness, we take $k = 1$. The first Fourier coefficient of u is then given by

$$\hat{u}_1 = \hat{F}_1 e^{-ist},$$

so the equations for a and b become

$$\left. \begin{aligned} a_t &= -i \omega_a \overline{b \hat{F}_1} e^{ist}, \\ b_t &= -i \omega_b \overline{a \hat{F}_1} e^{ist}. \end{aligned} \right\} \quad (10)$$

For simplicity, let us pick the origin of time in such a way that \hat{F}_1 is real and negative. Then the equations in (10) have the particular family of solutions

$$a = \sqrt{\left| \frac{\beta}{\omega_b} \right|} J e^{i\alpha t}, \quad (11)$$

$$b = \gamma \sqrt{\left| \frac{\alpha}{\omega_a} \right|} \overline{J} e^{i\beta t}, \quad (12)$$

where α and β satisfy

$$\alpha + \beta = s \quad \text{and} \quad \alpha\beta = \omega_a \omega_b |\hat{F}_1|^2, \quad (13)$$

with $\gamma = \text{sign}(\alpha/\omega_a) = \text{sign}(\beta/\omega_b)$, and J an arbitrary complex constant.

Thus, Equation (1) becomes the O.D.E.

$$[-s + F(z)]F'(z) = 2\gamma|J|^2 |\hat{F}_1| \sin(z),$$

with solution

$$F(z) = s \pm 2|J| \sqrt{|\hat{F}_1| \sqrt{C - \gamma \cos(z)}}, \quad (14)$$

where $C \geq 1$ is a constant of integration. Notice that, if C is strictly larger than 1, the solution is smooth but, when $C = 1$, it develops a corner. In the latter case, the solution is

$$F(z) = s \pm 2|J| \sqrt{2|\hat{F}_1|} |\sin(z/2)|$$

when $\gamma = 1$, and

$$F(z) = s \pm 2|J| \sqrt{2|\hat{F}_1|} |\cos(z/2)|$$

when $\gamma = -1$. The value of s follows from equating the first Fourier mode of the solution to \hat{F}_1 , and imposing the requirement that F have zero mean. In the case with a corner, we have

$$\hat{F}_1 = \mp \gamma \frac{4\sqrt{2}}{3\pi} |J| \sqrt{|\hat{F}_1|} \quad \Rightarrow \quad \hat{F}_1 = -\frac{32|J|^2}{9\pi^2},$$

and

$$F(z) = s + \frac{16|J|^2}{3\pi} |\sin(z/2)| \quad \text{or} \quad F(z) = s - \frac{16|J|^2}{3\pi} |\cos(z/2)|. \quad (15)$$

Then, the condition that F have vanishing mean becomes

$$0 = \int_{-\pi}^{\pi} F(z) dz = 2\pi s + \gamma \frac{64|J|^2}{3\pi} \Rightarrow s = -\gamma \frac{32|J|^2}{3\pi^2}.$$

Now we may return to (13) and compute α and β ; they are

$$\alpha, \beta = \frac{16|J|^2}{3\pi^2} \left(-\gamma \pm \sqrt{1 - \frac{4\omega_a\omega_b}{9}} \right). \quad (16)$$

Notice that, because $\omega_a + \omega_b = -1$, $(\omega_a\omega_b) \leq 1/4$. Thus, α and β are always real.

Finally, from the definition of the invariant Q ,

$$Q = (\alpha - \beta)|J|^2.$$

This allows us to compute $|J|$ from the initial data,

$$|J|^4 = \pm \frac{3\pi^2}{32\sqrt{1 - \frac{4\omega_a\omega_b}{9}}} Q, \quad (17)$$

as well as determining which of the two solutions in (16) are α and β , depending on the sign of Q . The only remaining parameter in the exact solution is the sign of $\gamma = \pm 1$, which determines the orientation of the corner (upward or downward) as well as the direction of propagation of the traveling wave. Here, the situation depends rather strongly on the signs of ω_a and ω_b . When they are both negative, any sign of γ gives a solution, whereas, when they have opposite signs, only one choice of γ is consistent with a given sign of Q .

This can be explained in terms of a symmetry of the system in (1–3): Note that, when the signs of ω_a and ω_b are both negative, the equations remain invariant under the switch

$$a \rightarrow \sqrt{\frac{\omega_a}{\omega_b}} b,$$

$$b \rightarrow \sqrt{\frac{\omega_b}{\omega_a}} a,$$

which changes the sign of Q , while leaving u invariant. The equations are also invariant under the transformation

$$u(x) \rightarrow -u(-x),$$

$$a \rightarrow \sqrt{\frac{\omega_a}{\omega_b}} \bar{b},$$

$$b \rightarrow \sqrt{\frac{\omega_b}{\omega_a}} \bar{a},$$

which changes both the sign of Q and the orientation of possible corners in u . When one ω is positive, on the other hand, a similar symmetry does not seem to exist.

In the particular case when $\omega_a = \omega_b$, we are led to consider a symmetric solution with $u(x)$ odd and a and b real and equal. Adopting $k = 1$, and hence $\omega_a = -0.5$, we can write

$$\hat{u}_1 = -iS(t),$$

where

$$S(t) = \frac{1}{\pi} \int_0^\pi u(x, t) \sin(x) \, dx.$$

Then, the equations reduce to

$$u_t + \left(\frac{u^2}{2}\right)_x = 2a^2 \sin(x),$$

$$a_t = \frac{1}{2}a S.$$

These admit a particular solution of the form

$$u = \frac{1}{t - t_0} f(x), \quad (18)$$

$$a = \frac{1}{t - t_0} \frac{c}{\sqrt{2}}, \quad (19)$$

where $c > 0$ is a constant, $f(x)$ satisfies the O.D.E.

$$-f + \left(\frac{f^2}{2}\right)_x = c^2 \sin(x),$$

with $f(0) = 0$, $\hat{f}_1 = 2$ and a shock at $x = \pi$. The constant c follows from the constraint that $\hat{f}_1 = 2$. We show below that this particular solution is an attractor to all symmetric initial data.

Even for arbitrary ω , a weaker symmetry persists: solutions that start with $u(x)$ odd and a and b real remain that way. Note that such data exclude any traveling wave solution, because these do not preserve parity.

4. The numerical scheme

Because shocks are expected to play a central role in the dynamics of the model equations, it is important that their numerical solution make use of the conservation form of the equations. To this end, the amplitude of the nondispersive wave $u = u(x, t)$ is replaced by an array: $u = [u_1 \dots u_N]$, where $u_n = u_n(t)$ is the average of $u(x, t)$ over the n th cell [the interval of width $dx = 2\pi/N$, centered at $x_n = (n - 0.5)dx$].

The equations are then solved by a second-order Strang splitting algorithm [8], with one step solving the Burgers' equation via a second-order Godunov method and the other step solving the purely ODE part through a standard second-order Runge–Kutta.

With the interpretation of u_n as the average of u over the n th cell, the ODE part of the equation for u becomes:

$$\frac{du_n}{dt} = 2\operatorname{Re}(ik ab e^{-ikx_n}) \frac{2}{kdx} \sin\left(\frac{kdx}{2}\right) = -4\operatorname{Im}(ab e^{-ikx_n}) \frac{\sin(\frac{kdx}{2})}{dx},$$

where the extra factor $(2/(k dx)) \sin(k dx/2)$ arises from the averaging of e^{-ikx} over each cell. The correction brought about by this extra factor is at the same level as the second-order error in the scheme, so it is not really required. On the other hand, it involves so little extra work, that it seems worthwhile keeping, as we have done in the numerical calculations that follow.

5. Numerical results and discussion

5.1. Generic initial data and parameters

The first two sets of experiments are designed to study the behavior of the solutions to (1–3) with generic initial data. In the first set, the nondispersive wave $u(x, t)$ is the one unstable to the other two; whereas, in the second, it is the dispersive mode $b(t)$. In both cases, the initial data are

$$u(x, 0) = \Gamma[\sin(x) + 0.6 \cos(2x) - 0.4 \sin(2x) + 0.2 \sin(3x)],$$

$$a(0) = 1 + 0.2i,$$

$$b(0) = 0.75 + 0.5i,$$

where Γ is a tunable amplitude that distinguishes the various experiments within a set.

The frequencies are, for the first set,

$$\begin{aligned} k &= 1 & (u \text{ is the unstable wave}), \\ \omega_a &= -0.3, \\ \omega_b &= -0.7, \end{aligned}$$

and, for the second,

$$\begin{aligned} k &= 1, \\ \omega_a &= 0.5, \\ \omega_b &= -1.5 & (b \text{ is the unstable mode}). \end{aligned}$$

In both cases, we solve the system for the time interval $0 \leq t \leq 1,200$, with $n = 2,000$ spatial cells and a fixed Δt satisfying a conservative estimate for the CFL condition based on the initial data.

5.1.1. Experiments with u the unstable wave. The results of the first set of experiments with $\Gamma = 1$ and $\Gamma = 1/4$ are plotted in Figures 1 and 2, respectively. Figure 1A shows the energy E as a function of time which, after a sharp initial decay attributable to shocks, settles down to a nonzero value, precisely the one corresponding to the exact traveling wave solution (15) for the initial value of the Manley–Rowe invariant Q . Figure 1B shows snapshots of $u(x, t)$ at the initial time $t = 0$, intended to represent generic data, at an early time $t = 2$, when a strong shock is dominating the solution, and at the final time of the computation $t = 1200$, when the exact traveling wave solution has taken over. For comparison, this figure includes a plot of the exact solution (15), which agrees to a surprising degree with the numerical one, leaving little doubt that the final state of the experiment is, indeed, the exact traveling wave with a corner. Figures 1C and D and display the absolute values and actual complex amplitudes of a and b as functions of time, the former at the beginning and the latter only near the end of the computation. We see both dispersive waves converging very rapidly to their values in the exact solution (11, 12).

In Figure 2A, we see the evolution of $E(t)$ for the smaller amplitude $\Gamma = 1/4$. Although it also settles down to a final nonzero value, this is smaller than that of the exact traveling wave. Snapshots of $u(x, t)$ for various values of t (from $t = 1170$ to $t = 1200$), plotted in Figure 2B, show an evolving profile, where the wave shape seems to (almost) recur. This strongly suggests a quasiperiodic (in time) wave, one that undergoes a periodic deformation in shape as it travels. More evidence for this is given by Figure 2C, which

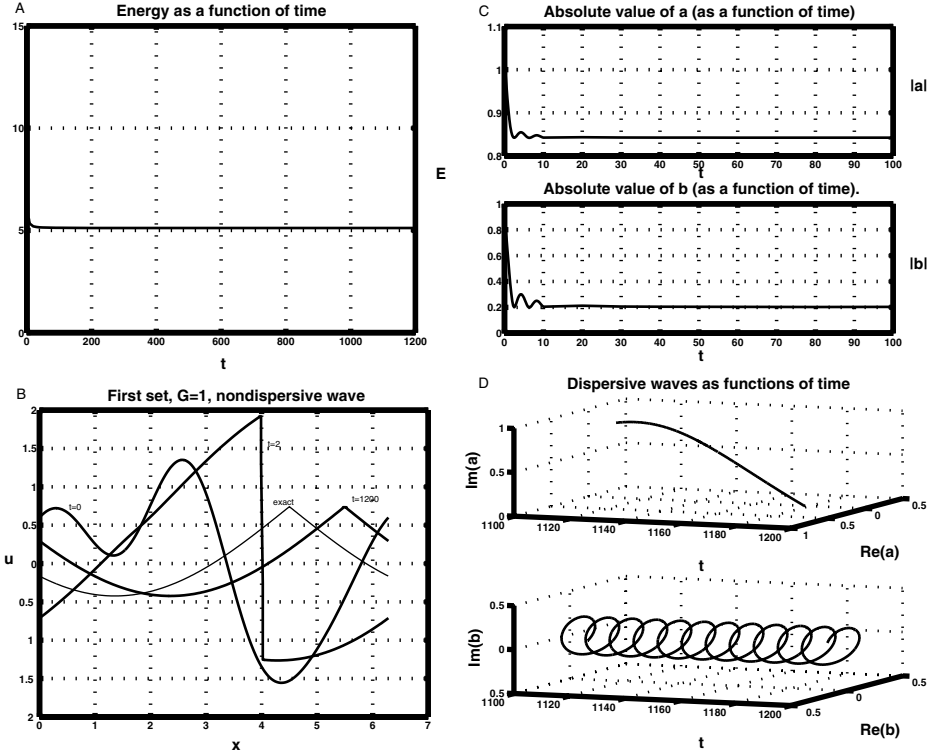


Figure 1. Solution to (1–3), with generic initial data and $u(x, t)$ the unstable wave. Specifically: $u(x, 0) = [\sin(x) + 0.6 \cos(2x) - 0.4 \sin(2x) + 0.2 \sin(3x)]$, $a(0) = 1 + 0.2 i$, and $b(0) = 0.75 + 0.5 i$, with frequencies $k = 1$, $\omega_a = -0.3$, and $\omega_b = -0.7$. Figure 1A shows the energy E settling down to the nonzero value (after a sharp initial decay attributable to shocks) corresponding to the traveling wave solution (15), with the Manley–Rowe invariant Q given by the initial data. Figure 1B shows snapshots of $u(x, t)$ at $t = 0$, at an early time $t = 2$ (a strong shock dominates the solution) and at the computation final time $t = 1200$ (the exact traveling wave solution has taken over). A plot of the exact solution (15) is included for comparison. Figures 1C and 1D display the absolute values and the complex amplitudes of a and b as functions of time. Both waves converge rapidly to the exact solution (11, 12). Figure 1D clearly shows b moving on a circle at a constant rate.

plots the norm of the change in shape as a function of time. The norm of the change in shape is defined by

$$\|u, u_0\|_{\text{shape}} = \min_{x_0} \|u(x) - u_0(x - x_0)\|_{\infty}, \quad (20)$$

where $u_0(x)$ is a reference profile; in our case $u_0(x) = u(x, 1100)$. Further evidence can be found in Figure 2D, which shows the late evolution of $|a(t)|$ and $|b(t)|$, periodic with a period different from (and in all likelihood incommensurable with) that of the phases of a and b (not displayed).

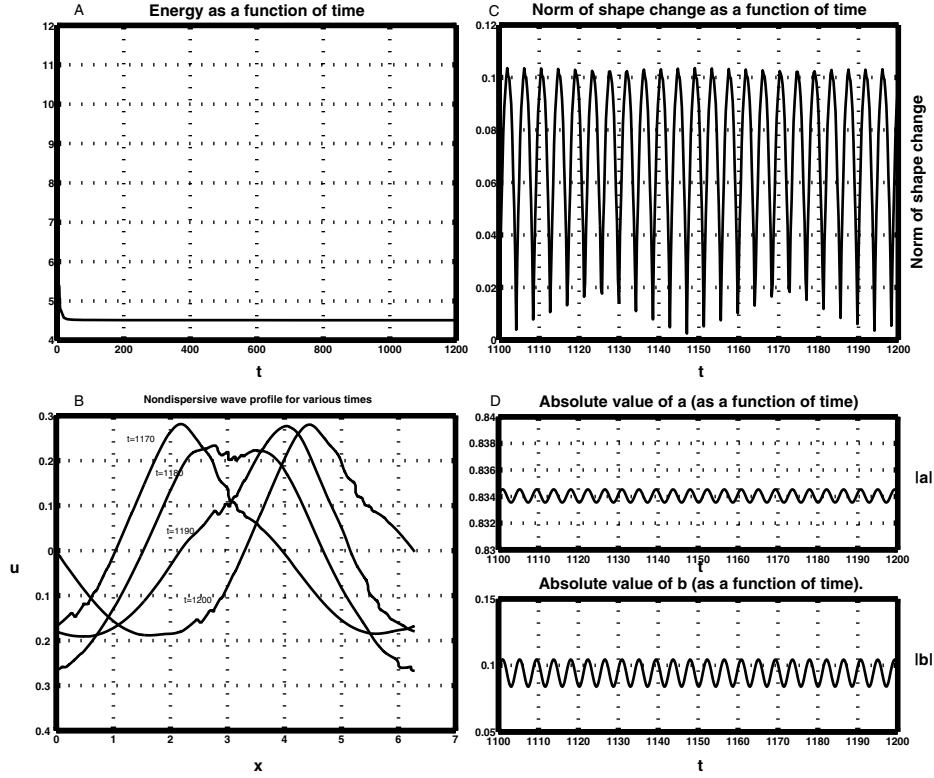


Figure 2. Solution to (1–3), with everything the same as in Figure 1; except for a smaller amplitude nondispersive wave: $u(x, 0) = 0.25 [\sin(x) + 0.6 \cos(2x) - 0.4 \sin(2x) + 0.2 \sin(3x)]$. Again, the energy E settles down to a final nonzero value (Figure 1A), but this value is smaller than that of the traveling wave. Snapshots of $u(x, t)$ for various values of t (Figure 2B) show an evolving profile with an (almost) recurrent wave shape. This suggests a quasiperiodic (in time) wave. Figure 2C shows a plot of the norm of the change in shape, as defined by (20). Finally, Figure 2D shows the late evolution of $|a(t)|$ and $|b(t)|$, periodic with a period different from that of the phases of a and b (not displayed).

Remark: In regard to the norm of the shape change in a solution, defined above in (20), note that when this norm vanishes, the solution is equal to the solution at the reference time, except for a space translation. In our numerical experiments, this norm quite never vanishes, but the observed behavior indicates that this may just be caused by lack of numerical resolution. For a given set of parameters, more points in the space grid and longer runs in time had the effect of producing closer approaches to zero in the shape norm. We hope that (future) more resolved runs will settle this question.

All these results are strongly reminiscent of those in [2] for a nondispersive wave interacting with a dispersive mode through topography, and in [3–6, 9] for

nondispersive waves interacting through either topography or a variable entropy. In all these cases, initial data with enough energy converge robustly to traveling waves with corners, and less energetic initial data, to smaller quasiperiodic waves. This is a very intriguing phenomena, which still awaits a full mathematical explanation.

5.1.2. Experiments with b the unstable wave. The situation in the second set of experiments, where the unstable wave is the dispersive mode b , is rather different. Figure 3A displays the profiles of $u(x, 1200)$ for three different values of Γ : 1/4, 2, and 8, together with the exact traveling wave solution corresponding to the value of the Manley–Rowe invariant Q common to the three runs. Neither of the three profiles agrees with this exact solution; in fact, the three of them seem to correspond to quasiperiodic waves. Figure 3B illustrates this for the case with $\Gamma = 8$, by plotting the norm of the change in shape of the solution. In fact, for $\Gamma = 2$ (and values nearby, which we have run but are not plotted here), the solution is relatively close to the exact traveling wave, although the sharp corner is entirely removed. However (unlike the cases where the unstable wave is u), as the initial energy of the runs gets larger, the final state gets smaller and further away from this exact solution.

5.2. Solutions with symmetries

It is interesting to observe the behavior of solutions with the symmetry $u(x, t)$ odd, $a(t)$ and $b(t)$ real, which excludes all traveling and most quasiperiodic waves. We first show the strongly symmetric case, where $\omega_a = \omega_b = -0.5$ and $a = b$. For example, consider the initial data

$$\begin{aligned} u(x, 0) &= \sin(x), \\ a(0) &= 1, \end{aligned}$$

and

$$b(0) = 1.$$

The numerical results converge very accurately to the exact self-similar solution (18, 19). Figure 4A shows the energy $E(t)$ rapidly converging to zero. Figure 4B includes two snapshots of $u(x, t)$ at the relatively late times $t = 350$ and $t = 700$, where the self-similarity of the solution becomes clear. Based on this (and other similar) experiments, it is natural to conjecture that almost all solutions with the strong symmetry u odd, $\omega_a = \omega_b$, a and b real and equal, will be attracted to this exact self-similar solution.

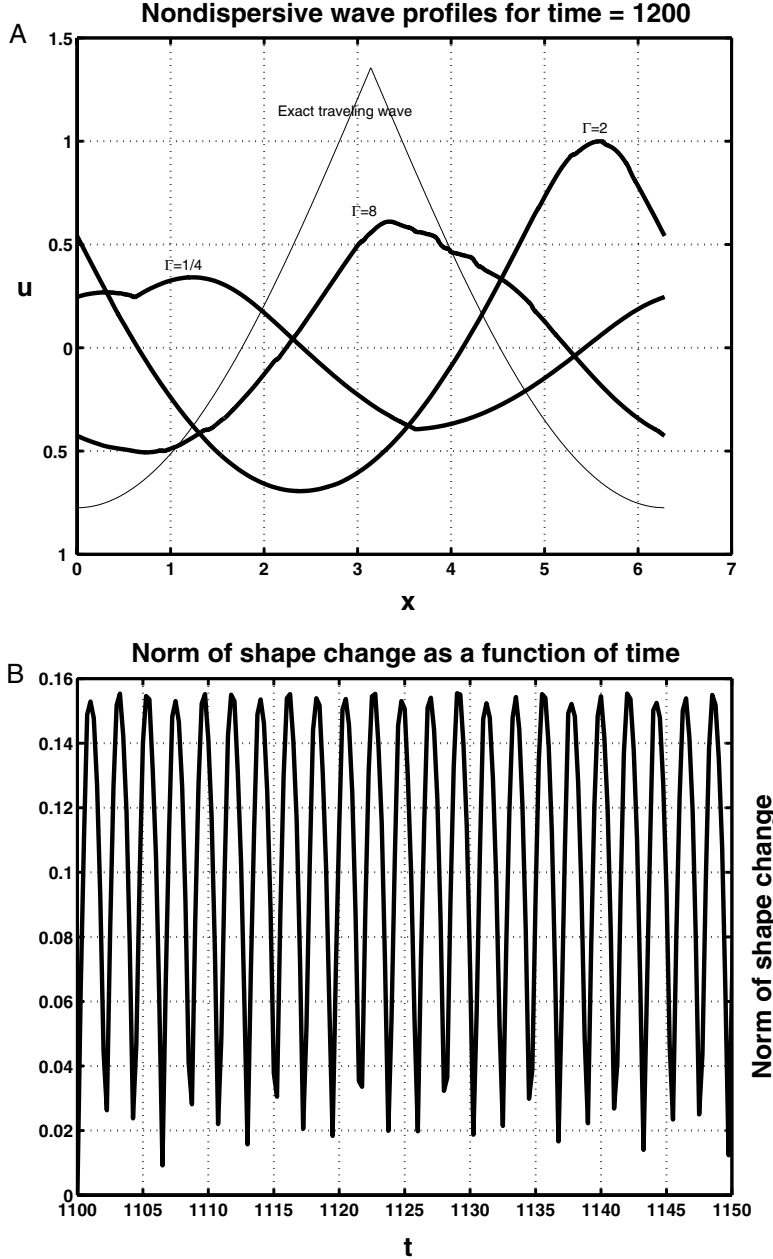


Figure 3. Solutions to (1–3), with generic initial data and b the unstable wave. For some $\Gamma > 0$: $u(x, 0) = \Gamma [\sin(x) + 0.6 \cos(2x) - 0.4 \sin(2x) + 0.2 \sin(3x)]$, $a(0) = 1 + 0.2 i$, and $b(0) = 0.75 + 0.5 i$, with frequencies $k = 1$, $\omega_a = 0.5$ and $\omega_b = -1.5$. Figure 3A displays the profiles of $u(x, 1200)$ for $\Gamma = 0.25, 2$ and 8 , together with the exact traveling wave solution (corresponding to the common value of the Manley–Rowe invariant \mathcal{Q}). Neither of the profiles agrees with this exact solution, and they all seem to correspond to quasiperiodic waves. Figure 3B illustrates this for the case with $\Gamma = 8$, by plotting the norm of the solution's change in shape. Unlike the cases where the unstable wave is u , as the initial energy gets larger, the final state gets smaller and farther away from the traveling wave solution.

5.3. Solutions with weak symmetries

Finally, we run a weakly symmetric case, where $\omega_a \neq \omega_b$, and b is the unstable wave. We take $\omega_a = 0.5$, $\omega_b = -1.5$ and the same initial data as above. The results are displayed in Figure 5. Figure 5A shows the absolute value of a approaching a nonzero constant; whereas b (slowly) decays to zero. Figure 5B includes two snapshots of $u(x, t)$ at relatively mature times, which show u converging to zero through permanent dissipation at two shocks, one at $x = 0$ and the other at $x = \pi$. Thus, the run seems to converge to a final state where only a is nonzero. This is consistent with the fact that b is the unstable mode, so it could not possibly stand alone. Nor could u stand alone, because it then would dissipate all its energy with shocks (moreover, a and b zero is not consistent with a nonzero Q). However, it is not clear to us why the solution needs to settle down to such simple configuration, with only one nonzero mode present.

6. Conclusions

The interactions between dispersive and nondispersive waves display an amazingly rich—and mostly unexplained—dynamics. Even the simplest model considered here, of a single nondispersive wave interacting with only two dispersive modes through a resonant triad, gives rise to surprising phenomena (such as the robust convergence of large enough initial data to a single traveling wave solution with a sharp corner). This single solution seems to be an attractor only when the frequency of the nondispersive mode has a sign opposite to the other two (u is unstable to a and b) and the initial energy is large enough. Otherwise, most initial data converge to quasiperiodic waves, with finite energy and no shocks.

Shock waves play an obviously prominent role in this selection mechanism; the corners in the final states are, in fact, leftovers from fully decayed shocks. How exactly shocks and triad resonances conspire to create this unique dynamic, however, remains mostly a mystery.

Acknowledgments

The work of R. R. Rosales was partially supported by NSF Grant DMS-9802713; the work of E. G. Tabak was partially supported by NSF Grant DMS-9501073; and the work of C. V. Turner was partially supported by Secyt-UNC Grant 275/98 and by CONICOR Grant 465/98. The authors thank A. J. Majda for pointing out that the equatorial waveguide might provide a scenario for resonances involving nondispersive waves.

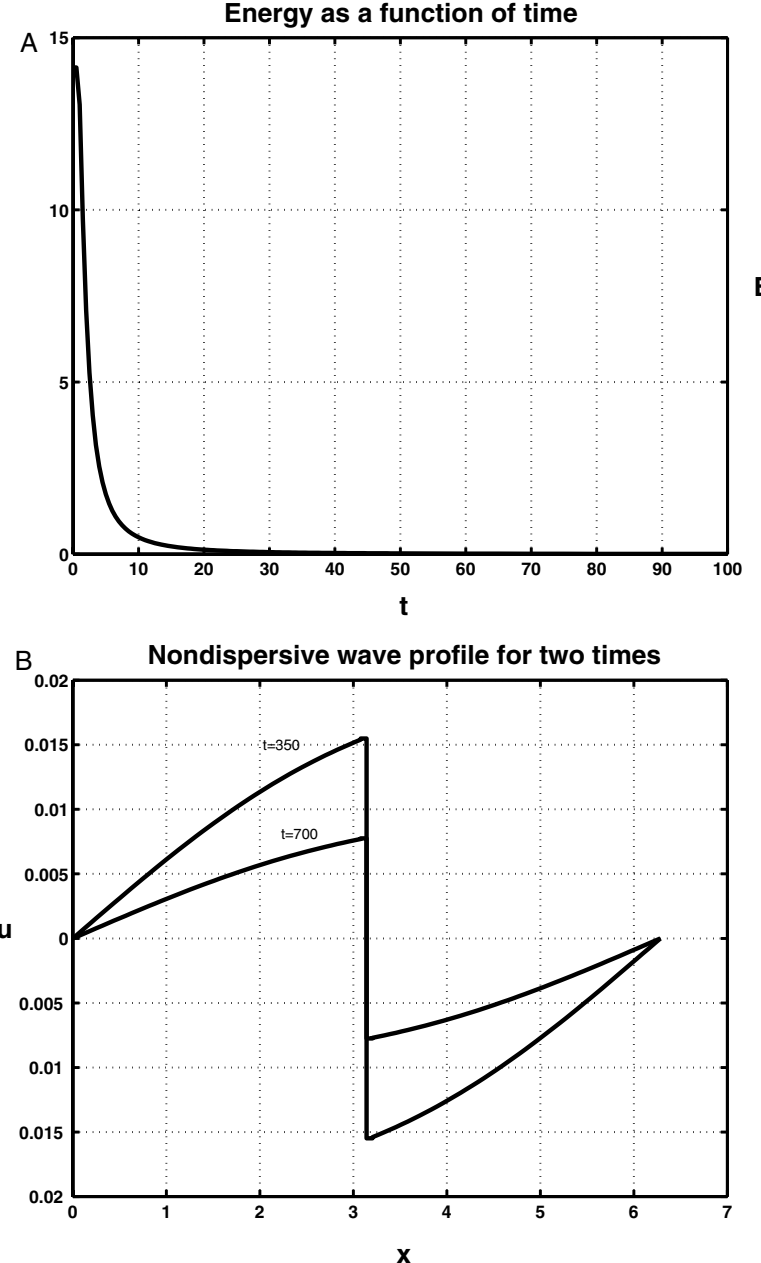


Figure 4. Solutions with the strong symmetry $u(x, t)$ odd, $a(t) = b(t)$ real and $\omega_a = \omega_b = -0.5$ ($k = 1$). Here, we take the initial data: $u(x, 0) = \sin(x)$ and $a(0) = b(0) = 1$. The solution converges very accurately to the exact self-similar solution (18,19). Figure 4A shows the energy $E(t)$ rapidly converging to zero. Figure 4B includes two snapshots of $u(x, t)$ at the late times $t = 350$ and $t = 700$, where the self-similarity of the solution becomes clear. We conjecture that almost all solutions with this strong symmetry will be attracted to the self-similar solution (18,19).

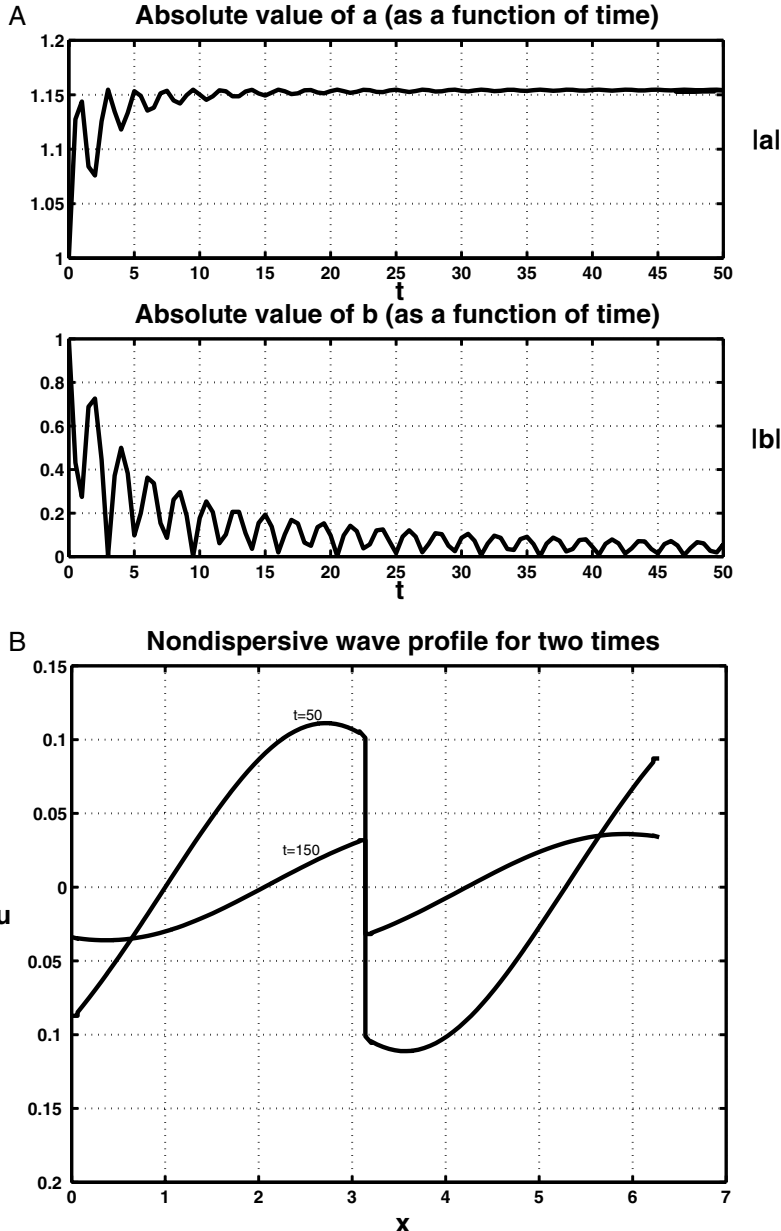


Figure 5. Solutions with the weak symmetry $u(x, t)$ odd, $a(t)$, and $b(t)$ real, but $\omega_a \neq \omega_b$. Here, we consider the case where b is the unstable wave (with $\omega_a = 0.5$, $\omega_b = -1.5$) and the same initial data as in Figure 4. Figure 5A shows the absolute value of a approaching a nonzero constant, while b (slowly) decays to zero. Figure 5B includes two snapshots of $u(x, t)$ at relatively mature times ($t = 50$ and $t = 150$), which show u converging to zero through permanent dissipation at two shocks, one at $x = 0$ and the other at $x = \pi$. Thus, the run seems to converge to a final state where only a is nonzero.

References

1. D. J. BENNEY and J. C. LUKE, Interactions of permanent waves of finite amplitude, *J. Math. Phys.* 43:309–313 (1964).
2. A. J. MAJDA, R. R. ROSALES, E. G. TABAK, and C. V. TURNER, Interaction of long-scale equatorial waves and dispersion of Kelvin waves through topographic resonances, *J. Atmos. Sci.* 56:4118–4133 (1999).
3. A. J. MAJDA, R. R. ROSALES, and M. SCHONBEK, A canonical system of integrodifferential equations arising in resonant nonlinear acoustics, *Stud. Appl. Math.* 79:205–262 (1988).
4. C. CELENTANO, Finite Amplitude Resonant Acoustic Waves Without Shocks, Ph.D. Thesis, MIT, Department of Mathematics, 1995.
5. D. VAYNBLAT, The Strongly Attracting Character of Large Amplitude Nonlinear Resonant Acoustic Waves Without Shocks, A Numerical Study. Ph.D. Thesis, MIT, Department of Mathematics, 1996.
6. M. SHEFTER, Never Breaking Quasiperiodic Solutions of Weakly Nonlinear Gas Dynamics, Ph.D. Thesis, MIT, Department of Mathematics, 1997.
7. L. SMITH and F. WALEFFE, Transfer of energy to two-dimensional large scales in forced, rotating, three-dimensional turbulence, *Phys. Fluids* 11:1608–1622 (1999).
8. G. STRANG, On the construction and comparison of difference schemes, *SIAM J. Num. Anal.* 5:506–517 (1968).
9. M. SHEFTER and R. ROSALES, Quasiperiodic solutions in weakly nonlinear gas dynamics. I. Numerical results in the inviscid case, *Stud. Appl. Math.* 103:279–337 (1999).

MASSACHUSETTS INSTITUTE OF TECHNOLOGY
 COURANT INSTITUTE OF MATHEMATICAL SCIENCES
 UNIVERSIDAD NACIONAL DE CÓRDOBA

(Received August 16, 2000)